Proceedings of
ASME Turbo Expo 2002
June 3–6, 2002, Amsterdam, The Netherlands

GT-2002-30314

DYNAMIC RESPONSE OF A HYDRODYNAMIC THRUST BEARING-MOUNTED ROTOR

T. N. Shiau , Professor*
K. S. Hsu Graduate*
and J. R. Chang Assistant Professor**
*Department of Mechanical Engineering
National Chung Cheng University
621 Chia Yi, Taiwan, R.O.C.
**Department of Mechanical Engineering
Nan-Jeon Institute of Technology
737 Tainan, Taiwan, R.O.C.

ABSTRACT

For investigating the dynamic response of a hydrodynamic thrust bearing-mounted flexible rotor, the dynamic characteristic data of thrust bearings for high surface velocities are applied for constructing the equation of motion for the rotor system, which is modeled with the finite element method (FEM). Based on the short bearing approximation and the π film cavitation model of the nonlinear oil-film forces, the dynamic responses are investigated using direct numerical integration with a variable order solver based on the numerical differentiation formulas (NDFs). Harmonic, quasi-periodic and chaotic motions are predicted for a range of spin speeds of the rotor. Poincaré maps of predicted rotor trajectories are also examined. It shows that spin speeds of the rotor and the oil film force coefficient might promote undesirable non-synchronous vibrations.

Keywords: Thrust bearing, Poincaré maps, Unbalance response, Quasi-periodic motions, and Chaotic motions.

INTRODUCTION

For safe operation of high-speed turbo-machinery, it is common practice to install squeeze film dampers to reduce the vibrations caused by unbalanced forces [1]. There has been much research focusing on the stability of the unbalanced response of rotors mounted in journal and squeeze film bearings. A non-synchronous mode of operation was mentioned by Mohan and Hahn [2]. Zhao et al. [3] had studied the stability of unbalanced responses of a squeeze film damped flexible rotor. Wang [4] applied an alternative method of finite elements in the time domain to predict the unbalanced response of rotor-bearing system using squeeze film dampers.

A high-speed rotor is usually equipped with a thrust bearing with two hydrodynamic oil films. Due to the relative motion of the thrust collar, both oil-films have a considerable effect on the lateral vibrations of the rotor-bearing system as presented by Mittwollen et al. [5] and Chen et al. [6]. The dynamic characteristics of hydrodynamic thrust bearing were presented by Storteig and White [7] and Ma et al. [8]. Jiang and Yu [9] provided an extensive theoretical investigation into the dynamic behavior of a rotor-bearing system equipped with a hydrodynamic thrust bearing.

Since axial thrust forces may be potentially damaging on the rotor-bearing system, it becomes necessary to consider these effects via thrust bearing on the rotor system motion. In this study, the effects of thrust bearing on shaft vibration are considered and applied to the system equation of motion. Harmonic, quasi-periodic and chaotic motions [10,11] are predicted for a range of spin speeds of the rotor by direct numerical integration. These motions can also be examined by Poincaré maps of the return points on the Phase Plane [10].

NOMENCLATURE

A	:	Cross-section area of the rotor
B	:	$B = \eta r L^3 / C_r^2$, oil film force parameter
$[C]$	:	Damping matrix of the system
C_r	:	Clearance of the bearing
E	:	Young's modulus of rotor shaft
$[F^L]$, $[F^N]$	:	System linear and nonlinear force vectors
$\overline{F}_{a,stat}$, $\overline{F}_{c,stat}$	:	Dimensionless static oil film forces on thrust pad on normal and tangential directions, respectively
F_x, F_y, F_z	:	Oil film forces on x, y and z directions, respectively
$[G]$	:	Gyroscopic matrix of the system
G	:	Shear modulus
I, I_d, I_p	:	Area moment of inertia of cross section of rotor and diametrical and polar mass moment of disk inertia, respectively
$[K]$	:	Stiffness matrix of the system
L	:	Thrust collar width
L_1, L_2	:	Length of each rotor element
$[M]$	:	Mass matrix of the system
M_B, M_Γ	:	Moments caused by oil film forces about y and z axes, respectively
$[Q(T)]$	:	Floquet transition matrix
T	:	A period T is $2\pi/\Omega$ when spin speed is Ω.
V, W	:	Nodal dimensionless translation displacements
$W_1(nT)$, $W_2(nT)$, $W_3(nT)$	:	The return points of nodes where the journal bearing, disk and thrust bearing are located
b	:	Thrust pad width
c_a, c_{BB}	:	Damping coefficients of thrust bearing
d_m	:	Mean diameter of thrust bearing
e	:	Disk eccentricity
f_v, f_w	:	Radial oil film forces acting on the bearing.
h_o	:	Thrust oil film thickness
k_a, k_{yB}, k_{BB}	:	Stiffness coefficients of thrust bearing
m_d	:	Mass of disk
l	:	Thrust pad length
$\{q\}$	:	Coordinate vectors for the system
r	:	Thrust collar radius
u, v, w, B, Γ	:	Nodal translation and rotation displacements
u_o	:	Static oil film thickness
z	:	Number of thrust pad
Λ_t	:	Eigen value of Floquet transition matrix
Ω	:	Spin speed of rotor
$\beta^*_{\alpha\alpha}$, $\gamma^*_{\alpha\alpha}$, $\gamma^*_{c\alpha}$	:	The dimensionless static and dynamic oil film force coefficients in axial and circumferential directions
η	:	Viscosity of lubricant

Hydrodynamic thrust bearing

The design of a hydrodynamic thrust bearing is shown in Fig. 1. Approximating the circular pad as a rectangle with length l and width b, as shown in Fig.2, the dimensionless static and dynamic oil film forces in axial and circumferential directions are functions of the dimensionless displacement of the thrust collar and can be represented as

$$\overline{F}_a = \overline{F}_{a,stat} + \Delta\overline{F}_a \tag{1}$$

$$\overline{F}_c = \overline{F}_{c,stat} + \Delta\overline{F}_c \tag{2}$$

where $\Delta\overline{F}_a = \gamma^*_{aa}\Delta\overline{u} + \beta^*_{aa}\Delta\overline{u}'$, $\Delta\overline{F}_c = \gamma^*_{ca}\Delta\overline{u}$ ($' = \partial/\partial\Omega t$). The coefficients, γ^*_{aa}, β^*_{aa} and γ^*_{ca}, and dimensionless forces, $\overline{F}_{a,stat}$ and $\overline{F}_{c,stat}$, have been determined by Mittwollen et al. [5].

For an axial displacement u_o of the thrust collar caused by an axial thrust force applying on the shaft, the static and dynamic oil film forces exerted on each side of the thrust collar, as shown in Fig. 3, can be represented as

$$F_a^r = F_{a,stat}^r + \Delta F_a^r \tag{3}$$

$$F_a^l = F_{a,stat}^l + \Delta F_a^l \tag{4}$$

Thus the total axial oil film forces acting on the thrust collar can be arranged as

$$F_x = F_a^l - F_a^r = -F_{a,stst} - k_a u - c_a \dot{u} \tag{5}$$

where $F_{a,stat}$, k_a and c_a are functions of axial displacement u_o of the thrust collar as given in APPENDIX A.

A change of the tilting angles (B,Γ) of the thrust collar changes the film thickness h_o of the single pad and therefore alters the axial and circumferential forces. Excluded the negligible reacting forces and momenta due to the radial movement of the thrust collar, as shown in Fig. 3, the reacting forces and momenta caused by the tilting angles (B,Γ) and titling angular velocities ($\dot{B}$,$\dot{\Gamma}$) can be determined. Combining the axial oil film force (F_x) and lateral nonlinear forces (f_v, f_w) caused by the radial oil film forces, the total reacting forces and momenta exerted on the thrust collar can be represented as

$$\begin{Bmatrix} F_x \\ F_y \\ F_z \end{Bmatrix} = \begin{bmatrix} -c_a & 0 & 0 \\ 0 & 0 & 0 \\ 0 & 0 & 0 \end{bmatrix} \begin{Bmatrix} \dot{u} \\ \dot{B} \\ \dot{\Gamma} \end{Bmatrix} + \begin{bmatrix} -k_a & 0 & 0 \\ 0 & k_{yB} & 0 \\ 0 & 0 & k_{yB} \end{bmatrix} \begin{Bmatrix} u \\ B \\ \Gamma \end{Bmatrix} + \begin{Bmatrix} F_{a,stat} \\ 0 \\ 0 \end{Bmatrix} + \begin{Bmatrix} 0 \\ f_v \\ f_w \end{Bmatrix} \tag{6}$$

$$\begin{Bmatrix} M_B \\ M_\Gamma \end{Bmatrix} = \begin{bmatrix} -k_{BB} & 0 \\ 0 & -k_{BB} \end{bmatrix} \begin{Bmatrix} B \\ \Gamma \end{Bmatrix} + \begin{bmatrix} -c_{BB} & 0 \\ 0 & -c_{BB} \end{bmatrix} \begin{Bmatrix} \dot{B} \\ \dot{\Gamma} \end{Bmatrix} \tag{7}$$

where k_{yB} , k_{BB}, and c_{BB} are functions of axial displacement u_o of the thrust collar as given in APPENDIX A. Ω is the spin speed of the rotor. And the lateral nonlinear oil film forces (f_v, f_w) are

$$f_v = -B\int_{\vartheta_1}^{\theta_2} \frac{(\dot{v}\cos\theta + \dot{w}\sin\theta)/C_r}{(1 - v\cos\theta/C_r - w\sin\theta/C_r)^3}\cos\theta d\theta \tag{8}$$

$$f_w = -B\int_{\vartheta_1}^{\theta_2} \frac{(\dot{v}\cos\theta + \dot{w}\sin\theta)/C_r}{(1 - v\cos\theta/C_r - w\sin\theta/C_r)^3}\sin\theta d\theta \tag{9}$$

where $B = \eta r L^3 / C_r^2$ and C_r is the radial clearance of the squeeze film damper. Using π film theory, $\phi = \tan^{-1}(\frac{w}{v})$, $\theta_2 = \tan^{-1}\frac{-\dot{v}}{\dot{w}}$, and $\theta_2 = \theta_1 + \pi$.

System equations of motion

The rotor system considered here, as shown in Fig. 4, consists of the following components: flexible shaft, unbalanced rigid disk, journal bearing and hydrodynamic thrust bearing. The system equations of motion are formulated by the finite element method and obtained by assembling the equations of motion of each component. They are given below

$$[M]\{\ddot{q}\} + ([C] - \Omega[G])\{\dot{q}\} + [K]\{q\} = \{F^L\} + \{F^N\} \qquad (10)$$

where $[M]$, $[C]$, $[G]$, $[K]$ are the mass, damping, gyroscopic and stiffness matrices of the system, respectively. $\{F^L\}$ and $\{F^N\}$ represent the system linear and nonlinear force vector, respectively. The nonlinear forces only act on the nonlinear supports where journal bearing and thrust bearing are installed. These coefficient matrices are as given in APPENDIX B.

Bifurcation diagram

A Poincaré section is a stroboscopic picture of a motion on a phase plane and it consists of the time series at a constant interval of T ($T=2\pi/\Omega$). The point on the Poincaré section is referred to as the return point. For the numerical computation of a bifurcation diagram, the rotor speed is increased in a constant step and the state variables at the end of the integration are used as initial values for the next speed. After reaching the steady state, the Z-coordinates ($W_1(nT)$, $W_2(nT)$, and $W_3(nT)$ for n=1 to 300) of the return points of consecutive 300 cycles at each node in the Poincaré section are then plotted versus the rotor speed.

Numerical examples and results

A high-speed rotor system, as shown in Fig.4, is employed to demonstrate the performance of the method. The corresponding configuration data of the thrust pad, rotor shaft and the disk are t_k=4.8x10^{-5}m, h_o=10^{-4}m, b=2.5x10^{-2}m, d_m=7.5x10^{-2}m, z=4, $l=\pi\ dm/4$, ρ=7680 kg/m^3, L_1=L_2=200mm, E=2.07x10^{11}N/m^2, G=7.96x10^{10} N/m^2, m_d=22kg, e=10^{-4}m, I_d=0.031 kgm^2, I_p=0.062 kgm^2, C_r=1mm. Due to the relative motion of the thrust collar, the effect of both oil-films on the lateral vibrations of the rotor-bearing system is first investigated. The coefficients of the thrust bearing are determined using various applied axial forces shown in Figs. 5&6. These results show that the stiffness coefficients k_a and k_{BB} increase as spin speed of the rotor increases and are independent of axial force, whereas k_{yB} increases as axial force increases and is independent of spin speed of the rotor. On the contrary, the damping coefficients c_a and c_{BB} decrease as spin speed of the rotor and little difference is observed with axial force variation. The results also show that the thrust bearing has little effect on the lateral damping coefficients.

Since the dynamic response will change with various oil film force coefficients B and different disk locations, these effects are first investigated by the bifurcation diagrams. The dimensionless displacement of response is defined as the radius of the orbit divided by radial clearance C_r of the bearing. The dimensionless Z-coordinates ($W_1(nT)$, $W_2(nT)$, and $W_3(nT)$) denote the return points at nodes where the journal bearing, disk and thrust bearing are located, respectively. They are plotted in the Poincaré section versus the rotor speeds with various oil film force coefficients B and different disk locations as shown in Figs. 7-10.

The distances of lengths are L_1=200 mm, L_2=200 mm for the case when the disk is located at the middle of the rotor. The bifurcation diagrams with B=100 and B=200 are plotted in Figs. 7& 8, respectively. The results show that chaotic motion occurs at higher spin speed and the spread of the return points is depressed when oil film force coefficient B gets larger. The distances of lengths are L_1=100 mm, L_2=300 mm and L_1=300 mm, L_2=100 mm for the cases when the disk is located near the left and right of the rotor, respectively. The bifurcation diagrams with various disk location when B=100 are plotted in Figs. 8-10, respectively. As compared from the results, the spread of the return points is depressed for the case when the disk is located near the right of the rotor where the thrust bearing is installed.

For the case when the disk is located at the middle of the rotor and the oil film force coefficient B is 200, the dynamic response is also examined. Harmonic, chaotic and quasi-periodic motions are predicted from the phase diagrams of the return points as shown in Figs. 11(a)-(d). For a harmonic motion, there will be only one mark on the phase diagram as shown in Fig. 11(a). By increasing the spin speed of the rotor further to 2270 rad/s and 2430 rad/s the responses tend to become chaotic as shown in Figs. 11(b) & (c). The quasi-periodic response results in closed orbits on Poincaré map as shown in Fig. 11(d).

Conclusions

In this paper, effects of a hydrodynamic thrust bearing on shaft vibration are employed to study the dynamic behavior of the rotor system. The results can be summarized as follows:

(1) The stiffness coefficients k_a and k_{BB} increase as spin speed of the rotor increases and are independent of axial force, whereas k_{yB} increases as axial force increases and is independent of spin speed of the rotor.
(2) The damping coefficients c_a and c_{BB} decrease as spin speed of the rotor and little difference is observed with axial force variation.
(3) The thrust bearing has more effects on the lateral stiffness coefficients than the lateral damping coefficients.
(4) Chaotic motion occurs at higher spin speed and the spread of the return points is depressed when oil film force coefficient B gets larger.
(5) The spread of the return points can be depressed when the disk is located near the thrust bearing.
(6) Harmonic, quasi-periodic and chaotic motions are predicted for a range of spin speeds of the rotor.

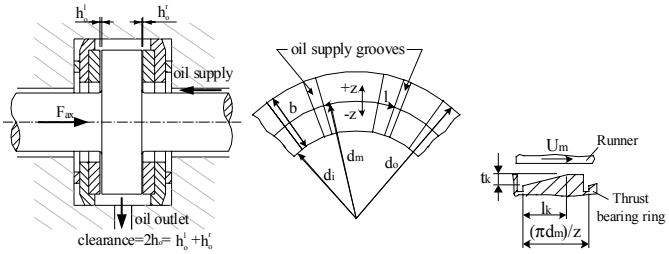

Fig. 1 Thrust bearing configuration [5]

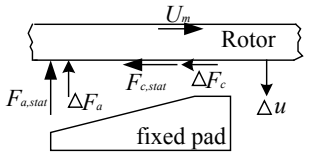

Fig. 2 Static and dynamic oil film forces [5]

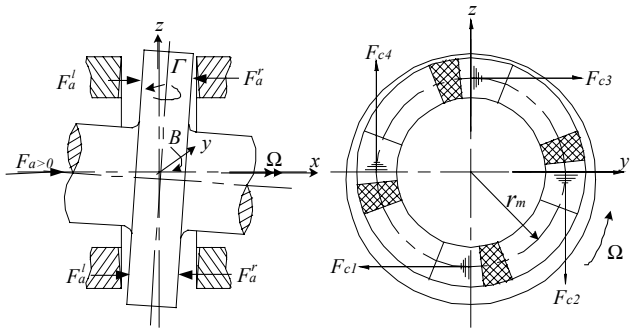

Fig. 3 Thrust bearing [5]

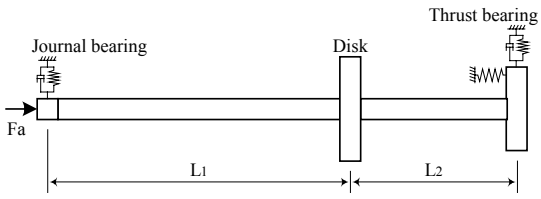

Fig.4(a) Configuration of a high-speed rotor system with a thrust bearing

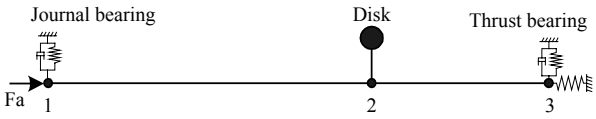

Fig.4(b) Finite Element Model of the system

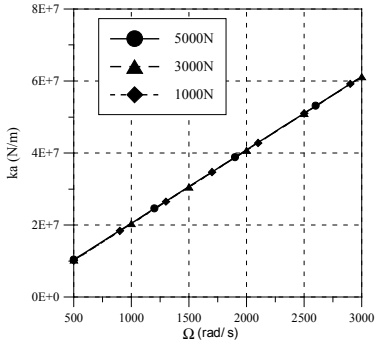

Fig. 5(a) Stiffness coefficients k_a v.s. Ω

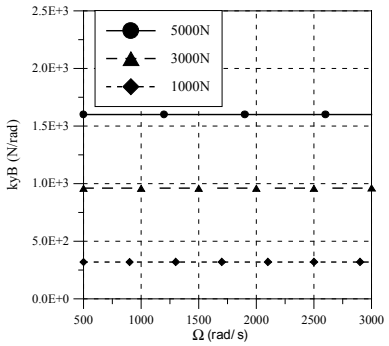

Fig. 5(b) Stiffness coefficients k_{yB} v.s. Ω

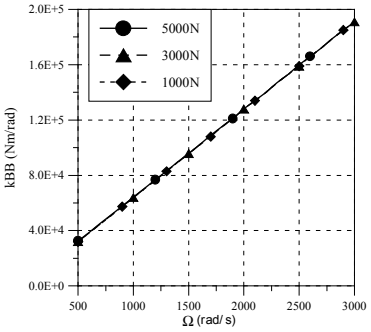

Fig. 5(c) Stiffness coefficients k_{BB} v.s. Ω

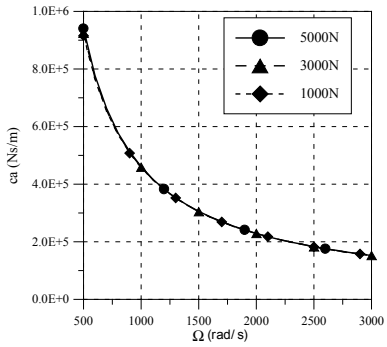

Fig. 6(a) Damping coefficients c_a v.s. Ω

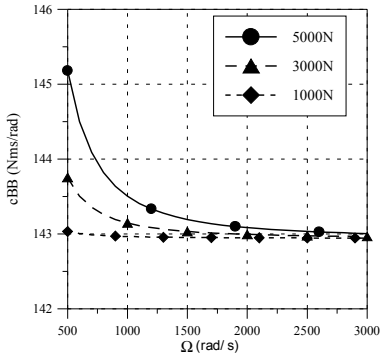

Fig. 6(b) Damping coefficients c_{BB} v.s. Ω

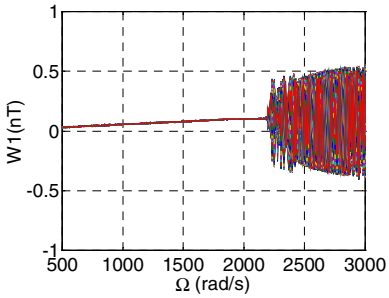

Fig. 7(a) Bifurcation diagram W_1(nT) of Journal bearing
(B=200, and disk is located at the middle of rotor).

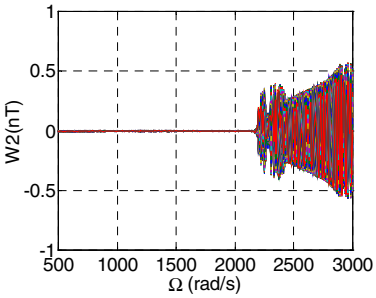

Fig. 7(b) Bifurcation diagram W_2(nT) of *Disk*
(B=200, and disk is located at the middle of rotor).

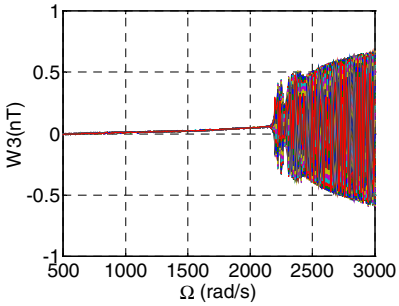

Fig. 7(c) Bifurcation diagram W_3(nT) of *Thrust bearing*
(B=200, and disk is located at the middle of rotor).

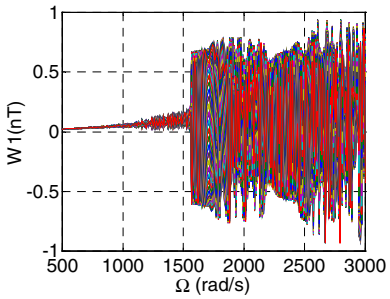

Fig. 8(a) Bifurcation diagram W_1(nT) of *Journal bearing*
(B=100, and disk is located at the middle of rotor).

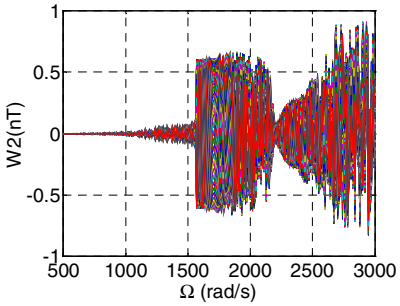

Fig. 8(b) Bifurcation diagram W_2(nT) of *Disk*
(B=100, and disk is located at the middle of rotor).

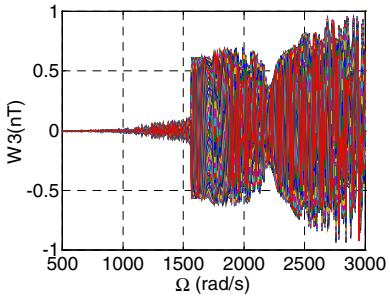

Fig. 8(c) Bifurcation diagram W_3(nT) of *Thrust bearing*
(B=100, and disk is located at the middle of rotor).

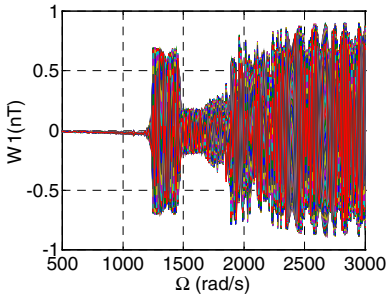

Fig. 9(a) Bifurcation diagram W_1(nT) of *Journal bearing*
(B=100, and disk is located near the left of rotor).

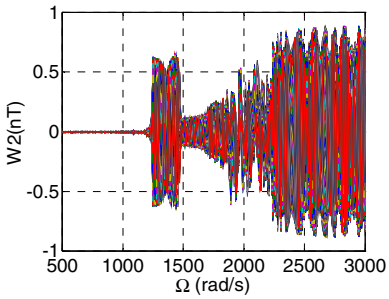

Fig. 9(b) Bifurcation diagram W_2(nT) of *Disk* (B=100, and disk is located near the left of rotor).

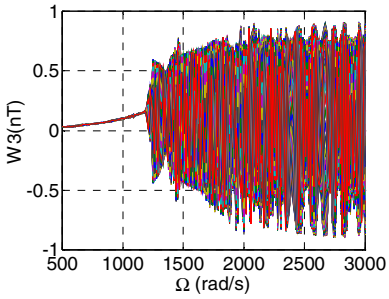

Fig. 9(c) Bifurcation diagram W_3(nT) of *Thrust bearing* (B=100, and disk is located near the left of rotor).

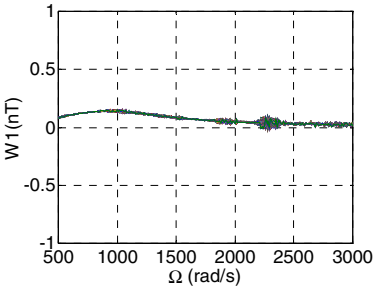

Fig. 10(a) Bifurcation diagram W_1(nT) of *Journal bearing* (B=100, and disk is located near the right of rotor).

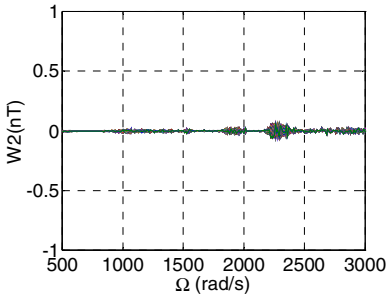

Fig. 10(b) Bifurcation diagram W_2(nT) of *Disk* (B=100, and disk is located near the right of rotor).

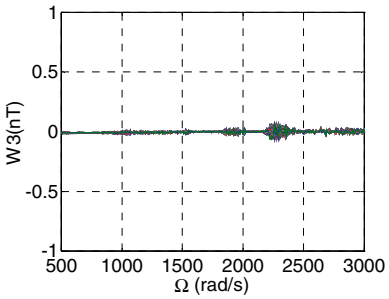

Fig. 10(c) Bifurcation diagram W_3(nT) of *Thrust bearing* (B=100, and disk is located near the right of rotor).

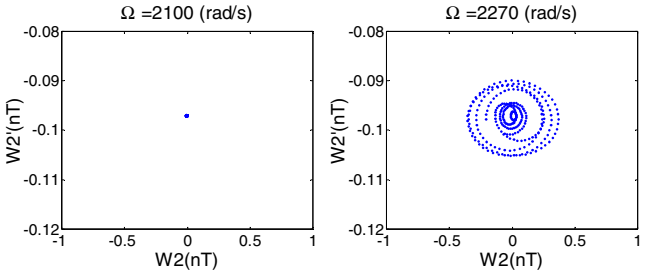

(a) harmonic motion (b) chaotic motion

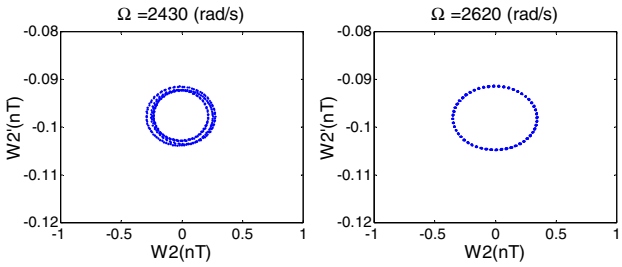

(c) chaotic motion (d) quasi-periodic motion

Fig. 11 Phase diagram of of W_2(nT) at various Ω

References

[1] Holmes, R., 1985, "The Control of Engine Vibration Using Squeeze Film Dampers," ASME *Journal of Engineering for Power*, **105**, pp. 525-529.

[2] Mohan, S., and Hahn, E. J., Aug. 1974, "Design of Squeeze-Film Damper Supports for Rigid Rotors," ASME *Journal of Engineering for Industry*, **96**, No. 3, pp. 976-982.

[3] Zhao, J. Y., Linnett, I. W. and McLean, L. J., April 1994, " Stability and Bifurcation of Unbalanced Response of a Squeeze Film Damped Flexible Rotor," ASME *Journal of Tribology*, **116**, pp. 361-368.

[4] Wang, Y., July 1997, " Prediction of Periodic Response of Rotor Dynamic Systems With Nonlinear Supports," ASME *Journal of Vibration*, *Acoustics*, **119**, pp.346-353.

[5] Mittwollen, N., Hegel, T. and Glienicke, J., OCT. 1991, " Effect of Hydrodynamic Thrust Bearings on Lateral Shaft

Vibrations," ASME *Journal of Tribology*, **113**, No.4, pp. 811-818.

[6] Chen, W., Glienicke, J. and Zhu, J., Oct. 1992, "The Effect of the Thrust Bearing on the Bending Vibration State of a Single-Mass Rotor," *Journal of XiAnJiaotong University*, **26**, No.5, pp.11-18.

[7] Storteig, E. and White, M. F., 1999, " Dynamic Characteristics of Hydro-dynamically Lubricated Fixed-Pad Thrust Bearing," *Wear*, **232**, pp.250-255.

[8] Ma, X. Z., Zhang, G. X. and Zhu, J., Aug. 2000, " Calculation and Analysis on Dynamic Coefficients of Circular Pivot-pad Thrust Bearing," *Tribology*, **20**, No.4, pp. 300-303.

[9] Jiang, P. L., and Yu, L., 1999, " Dynamics of a Rotor-Bearing System Equipped With a Hydrodynamic Thrust Bearing," *Journal of Sound and Vibration*, **227**, pp.863-872.

[10] Shiau, T. N., Rao, J. S., Chang, J. R. and Choi, S. T., 1999, " Dynamic Behavior of Geared Rotors," ASME *Journal of Engineering for Gas Turbine and Power*, **121**, No.3, pp. 494-503.

[11] Shiau, T.N., Chang, J.R., and Choi, S.T., 2001, "Stability Analysis of a Gear Pair System Supported by Squeeze-Film Dampers," *International Journal of Rotating Machinery*, **7**, No. 2, pp. 143-151.

APPENDIX A The static force and coefficients for thrust bearing

$$F_{a,stat} = \Omega\left(\frac{\overline{F}^{\,l}_{a,stat}\left(\frac{h_o+u_o}{t_k}\right)}{(h_o+u_o)^2} - \frac{\overline{F}^{\,r}_{a,stat}\left(\frac{h_o-u_o}{t_k}\right)}{(h_o-u_o)^2}\right) bl^2\,\tfrac{d_m}{2}\eta + \Omega k_a u_o \tag{11}$$

$$k_a = \Omega\left(\frac{\gamma^*_{aa}\left(\frac{h_o-u_o}{t_k}\right)}{(h_o-u_o)^3} + \frac{\gamma^*_{aa}\left(\frac{h_o+u_o}{t_k}\right)}{(h_o+u_o)^3}\right) bl^2\,\tfrac{d_m}{2}\eta \tag{12}$$

$$c_a = \left(\frac{\beta^*_{aa}\left(\frac{h_o-u_o}{t_k}\right)}{(h_o-u_o)^3} + \frac{\beta^*_{aa}\left(\frac{h_o+u_o}{t_k}\right)}{(h_o+u_o)^3}\right) bl^3\eta \tag{13}$$

$$k_{yB} = \Omega\left(\frac{\gamma^*_{ca}\left(\frac{h_o-u_o}{t_k}\right)}{(h_o-u_o)^2} - \frac{\gamma^*_{ca}\left(\frac{h_o+u_o}{t_k}\right)}{(h_o+u_o)^2}\right) \frac{bl\eta z(d_m^2+b^2)}{8} \tag{14}$$

$$k_{BB} = \Omega\left(\frac{\gamma^*_{aa}\left(\frac{h_o-u_o}{t_k}\right)}{(h_o-u_o)^3} + \frac{\gamma^*_{aa}\left(\frac{h_o+u_o}{t_k}\right)}{(h_o+u_o)^3}\right) \frac{d_m bl^2\eta z(d_m^2+b^2)}{16} \tag{15}$$

$$c_{BB} = \left(\frac{\beta^*_{aa}\left(\frac{h_o-u_o}{t_k}\right)}{(h_o-u_o)^3} + \frac{\beta^*_{aa}\left(\frac{h_o+u_o}{t_k}\right)}{(h_o+u_o)^3}\right) \frac{bl^3\eta z(d_m^2+b^2)}{8} \tag{16}$$

APPENDIX B Coefficient matrices of the system

$$\{q\} = \{u_1 \;\; v_1 \;\; w_1 \;\; B_1 \;\; \Gamma_1 \;\; u_2 \;\; v_2 \;\; w_2 \;\; B_2 \;\; \Gamma_2 \;\; u_3 \;\; v_3 \;\; w_3 \;\; B_3 \;\; \Gamma_3\}^T \tag{17}$$

$$\{F^L\} = \{F_a \;\; 0 \;\; 0 \;\; 0 \;\; 0 \;\; 0 \;\; m_d e\cos\Omega t \;\; m_d e\sin\Omega t \;\; 0 \;\; 0 \;\; -F_a \;\; 0 \;\; 0 \;\; 0 \;\; 0\}^T \tag{18}$$

$$\{F^N\} = \{0 \;\; f_{v1} \;\; f_{w1} \;\; 0 \;\; 0 \;\; 0 \;\; 0 \;\; 0 \;\; 0 \;\; 0 \;\; 0 \;\; f_{v3} \;\; f_{w3} \;\; 0 \;\; 0\}^T \tag{19}$$

$$[M] = [M_{i,j}] = [M_{j,i}],$$

where

$$\begin{aligned}
&M_{1,1} = 2M_{6,1} = \rho AL_1/3, M_{6,6} = \rho A(L_1+L_2)/3 + m_d,\\
&M_{11,11} = 2M_{11,6} = \rho AL_2/3,\\
&M_{2,2} = M_{3,3} = m_{11}, M_{5,2} = -M_{4,3} = -m_{21}, M_{4,4} = M_{5,5} = m_{31},\\
&M_{7,2} = M_{8,3} = m_{41}, M_{7,5} = -M_{8,4} = M_{9,3} = -M_{10,2} = m_{51},\\
&M_{9,4} = M_{10,5} = -m_{61}, M_{7,7} = M_{8,8} = m_{11} + m_{12} + m_d,\\
&M_{9,9} = M_{10,10} = m_{31} + m_{32} + I_d, M_{9,8} = -M_{10,7} = m_{21} - m_{22},\\
&M_{12,7} = M_{13,8} = m_{42}, M_{12,10} = -M_{13,9} = M_{14,8} = -M_{15,7} = m_{52},\\
&M_{14,9} = M_{15,10} = -m_{62}, M_{12,12} = M_{13,13} = m_{12}, M_{14,13} = -M_{15,12} = m_{22},\\
&M_{14,14} = M_{15,15} = m_{32}, others = 0.
\end{aligned} \tag{20}$$

$$[C] = [C_{i,j}], C_{11,11} = c_a, C_{14,14} = c_{BB}, C_{15,15} = c_{BB}, others = 0. \tag{21}$$

$$[G] = [G_{i,j}] = -[G_{j,i}],$$

where

$$\begin{aligned}
&G_{3,2} = G_{7,3} = -G_{8,2} = g_{11}, G_{4,2} = G_{5,3} = G_{7,4} = G_{8,5} = G_{9,2} = G_{10,3} = g_{21},\\
&G_{5,4} = g_{31}, G_{9,5} = -G_{10,4} = g_{41}, G_{8,7} = g_{11} + g_{12}, G_{9,7} = G_{10,8} = -g_{21} + g_{22},\\
&G_{10,9} = g_{31} + g_{32} - I_p, G_{12,8} = -G_{13,7} = g_{12},\\
&G_{12,9} = G_{13,10} = G_{14,7} = G_{15,8} = -G_{14,12} = -G_{15,13} = g_{22},\\
&G_{14,10} = -G_{15,9} = g_{42}, G_{13,12} = g_{12}, G_{15,14} = g_{32}, others = 0.
\end{aligned} \tag{22}$$

$$[K] = [K^1] + [K^2] \tag{23}$$

$$[K^1] = [K^1_{i,j}] = [K^1_{j,i}],$$

where

$$\begin{aligned}
&K^1_{1,1} = -K^1_{6,1} = EA/L_1, K^1_{6,6} = EA/L_1 + EA/L_2, K^1_{11,11} = -K^1_{11,6} = EA/L_2,\\
&K^1_{2,2} = K^1_{3,3} = -K^1_{7,2} = -K^1_{8,3} = k_{11},\\
&K^1_{5,2} = -K^1_{4,3} = -K^1_{7,5} = K^1_{8,4} = -K^1_{9,3} = K^1_{10,2} = k_{31},\\
&K^1_{4,4} = K^1_{5,5} = k_{21}, K^1_{9,4} = K^1_{10,5} = k_{41}, K^1_{7,7} = K^1_{8,8} = k_{11} + k_{12},\\
&K^1_{9,9} = K^1_{10,10} = k_{21} + k_{22}, K^1_{12,12} = K^1_{13,13} = -K^1_{12,7} = -K^1_{13,8} = k_{12},\\
&K^1_{9,8} = -K^1_{8,7} = k_{31} - k_{32}, K^1_{15,7} = -K^1_{14,8} = K^1_{13,9} = K^1_{14,13} = -K^1_{15,12} = k_{32},\\
&K^1_{14,9} = K^1_{15,10} = k_{42}, K^1_{14,14} = K^1_{15,15} = k_{22}, others = 0.
\end{aligned} \tag{24}$$

$$[K^2] = [K^2_{i,j}], \tag{25}$$

where

$$K^2_{11,11} = k_a, K^2_{12,14} = -k_{yB}, K^2_{13,15} = -k_{yB}, K^2_{14,14} = k_{BB}, K^2_{15,15} = k_{BB}, others = 0.$$

where i=1,2 for each following term.

$$\Phi_i = \frac{12EI}{kGAL_i^2},\ \Xi_{1i} = \frac{\rho AL_i}{420(1+\Phi_i)^2},\ \Xi_{2i} = \frac{\rho AI}{30L_i(1+\Phi_i)^2},\ \Xi_{3i} = \frac{-\rho I}{15L_i(1+\Phi_i)},$$

$$\Xi_{4i} = \frac{F_a}{30L_i(1+\Phi_i)^2},\ \Xi_{5i} = \frac{EI}{L_i^3(1+\Phi_i)}.$$

$$m_{1i} = (156 + 294\Phi_i + 140\Phi_i^2)\Xi_{1i} + 36\Xi_{2i}$$

$$m_{2i} = (22 + 38.5\Phi_i + 17.5\Phi_i^2)L_i\Xi_{1i} + (3 - 15\Phi_i)L_i\Xi_{2i}$$

$$m_{3i} = (4 + 7\Phi_i + 3.5\Phi_i^2)L_i^2\Xi_{1i} + (4 + 5\Phi_i + 10\Phi_i^2)L_i^2\Xi_{2i}$$

$$m_{4i} = (54 + 126\Phi_i + 70\Phi_i^2)\Xi_{1i} - 36\Xi_{2i}$$

$$m_{5i} = (13 + 31.5\Phi_i + 17.5\Phi_i^2)L_i\Xi_{1i} - (3 - 15\Phi_i)L_i\Xi_{2i}$$

$$m_{6i} = (3 + 7\Phi_i + 3.5\Phi_i^2)L_i^2\Xi_{1i} + (1 + 5\Phi_i - 5\Phi_i^2)L_i^2\Xi_{2i}$$

$$g_{1i} = 36\Xi_{3i}\,,\; g_{2i} = (-3 + 15\Phi_i)L_i\Xi_{3i}\,,\; g_{3i} = (4 + 5\Phi_i + 10\Phi_i^2)L_i^2\Xi_{3i}$$

$$g_{4i} = (1 + 5\Phi_i - 5\Phi_i^2)L_i^2\Xi_{3i}\,,\; k_{1i} = (36 + 60\Phi_i + 30\Phi_i^2)\Xi_{4i} + 12\Xi_{5i}$$

$$k_{2i} = (4 + 5\Phi_i + 2.5\Phi_i^2)L_i^2\Xi_{4i} + (4 + \Phi_i)L_i^2\Xi_{5i}\,,\; k_{3i} = 3L_i\Xi_{4i} + 6L_i\Xi_{5i}$$

$$k_{4i} = (-1 - 5\Phi_i - 2.5\Phi_i^2)L_i^2\Xi_{4i} + (2 - \Phi_i)L_i^2\Xi_{5i}$$